JACS
JOURNAL OF THE AMERICAN CHEMICAL SOCIETY
pubs.acs.org/JACS
Communication

Controlling the Direction of *S*-Nitrosation versus Denitrosation: Reversible Cleavage and Formation of an S−N Bond within a Dicopper Center

Wenjie Tao, Alina Yerbulekova, Curtis E. Moore, Hannah S. Shafaat,* and Shiyu Zhang*

Cite This: *J. Am. Chem. Soc.* 2022, 144, 2867−2872
Read Online
ACCESS | Metrics & More | Article Recommendations | Supporting Information

ABSTRACT: Iron and copper enzymes are known to promote reversible *S*-nitrosation/denitrosation in biology. However, it is unclear how the direction of S−N bond formation/scission is controlled. Herein, we demonstrate the interconversion of metal-*S*-nitrosothiol adduct M(RSNO) and metal nitrosyl thiolate complex M(NO)(SR), which may regulate the direction of reversible *S*-(de)nitrosation. Treatment of a dicopper(I,I) complex with RSNO leads to a mixture of two structural isomers: dicopper(I,I) *S*-nitrosothiol $[Cu^{I}Cu^{I}(RSNO)]^{2+}$ and dicopper(II,II) nitrosyl thiolate $[Cu^{II}Cu^{II}(NO)(SR)]^{2+}$. The K_{eq} between these two structural isomers is sensitive to temperature, the solvent coordination ability, and counterions. Our study illustrates how copper centers can modulate the direction of RS−NO bond formation and cleavage through a minor perturbation of the local environment.

S-Nitrosation (or *S*-nitrosylation) is an important post-translational modification in which the thiol functional group in cysteine (Cys) is converted to *S*-nitrosothiol (RSNO).[1−8] The reversible conversion of CysS−H to CysS−NO has been proposed to involve important biological processes, such as the autoregulation of blood flow[9−12] and the proper functioning of mitochondria.[13] *S*-Nitrosation reactions in biology are often reversible,[3,5] providing a flexible strategy for modifying protein structures with NO•. Both *S*-nitrosation and denitrosation can be mediated by iron,[14−21] copper,[22−26] and other metals.[27−29] However, the factors governing the direction of *S*-nitrosation vs denitrosation at metal centers remain underexplored. For example, it is unclear why certain copper proteins promote RS−NO bond formation[22,23] while others promote NO• release from RS−NO.[30,31]

Among the reports of metal-mediated *S*-(de)nitrosation, two examples are fully reversible.[16,25,26] Montfort et al. demonstrated that the ferric (Fe^{III}) heme iron site in nitrophorin reacts with NO• to afford nitrosated cysteinate along with a heme [FeNO]^{7} center (Scheme 1A).[16] This Fe-mediated *S*-nitrosation process is reversed over time, releasing NO• and regenerating the Fe^{III} heme center. Similarly, type 1 copper (T1) sites can reversibly store NO• by converting the CysS−Cu^{II} motif to CysS−NO with the simultaneous reduction of Cu^{II} to Cu^{I} (Scheme 1B).[26] A modeling study has shown that purging a solution of the Cu^{I}(RSNO) complex with a stream of N_2 promotes the release of NO• and regenerates the Cu^{II}−thiolate complex.[25] In addition to mononuclear Cu and Fe sites, multinuclear metal centers, such as CuZn superoxide dismutase and ceruloplasmin (CP), are also closely associated with the storage[22,23] and release[30,31] of NO• as RSNO. Akaike et al. found that the RSNO-generation activity of CP was significantly suppressed by inhibitors of type 2 copper (T2) and binuclear type 3 copper (T3) sites, e.g., azide, cyanide, and fluoride,[22] suggesting that trinuclear copper centers may be

Scheme 1

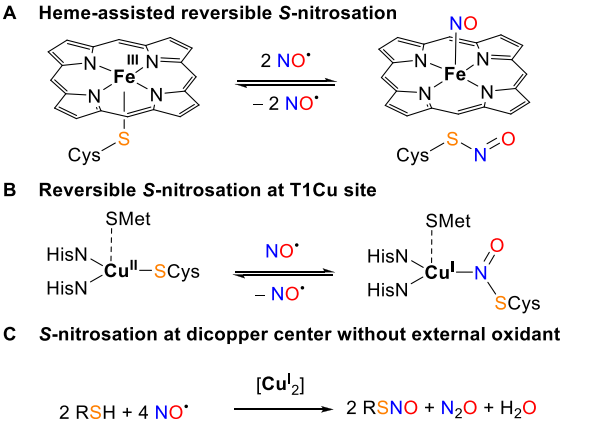

associated with the conversion of NO• and RSH to RSNO. Recently, we demonstrated that a synthetic dicopper complex could promote *S*-nitrosation without an external oxidant, which serves as a functional model of ceruloplasmin-mediated NO• storage (Scheme 1C).[32,33]

A common mechanistic step in metal-mediated *S*-nitrosation is the insertion of NO• into metal−thiolate bonds to generate RSNO together with the reduced metal center,[16,25,26,28] reminiscent of reductive elimination in organometallic chemistry. Therefore, it is commonly proposed that the coupling of NO• with thiol occurs at a transient metal nitrosyl

Received: December 5, 2021
Published: February 9, 2022

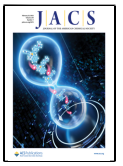

https://doi.org/10.1021/jacs.1c12799
J. Am. Chem. Soc. 2022, 144, 2867−2872

thiolate species $M_x(NO)(SR)$ (Scheme 2A), which undergoes reductive elimination to afford $M_x(RSNO)$.[20,25,28] The reverse

Scheme 2

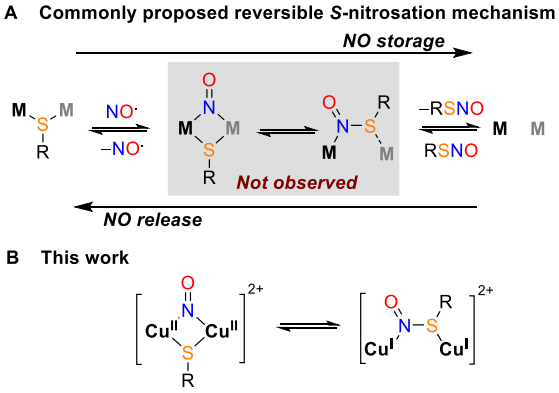

reaction—a formal oxidative addition of RSNO—promotes the release of NO•. If this interconversion is possible, then the chemical factors that govern the equilibrium between $M_x(NO)(SR)$ and $M_x(RSNO)$ could be the key to understanding how biological metal centers control the direction of *S*-nitrosation vs denitrosation.

Herein, we demonstrate the reversible interconversion between $M_2(NO)(SR)$ and $M_2(RSNO)$ (Scheme 2B). Unprecedented Cu(II,II) μ-NO μ-thiolate $[Cu^{II}_2(NO)(SR)]$ complex **3** and its structural isomer Cu(I,I) *S*-nitrosothiol $[Cu^{I}_2(RSNO)]$ complex **2** were fully characterized with spectroscopy or single-crystal X-ray crystallography. In solution, these two isomers coexist in equilibrium, and K_{eq} varies as a function of temperature, solvent coordination ability, and counterions. The reversible conversion between $M_2(NO)(SR)$ and $M_2(RSNO)$ represents a potentially pivotal mechanistic step that controls the directionality of RS–NO bond cleavage and formation in biology.

To visualize the interconversion between $M_x(NO)(SR)$ and $M_x(RSNO)$, we employ our dicopper platform[33] which has successfully modeled the *S*-nitrosation process at ceruloplasmin.[22,23] Instead of using the previous Py_4DMB ligand (Scheme 3 right), we prepared a new binucleating ligand **L**

Scheme 3. Comparison of L and Py_4DMB

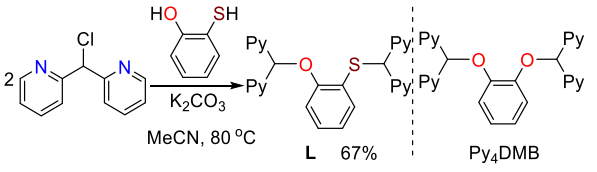

by linking four pyridines with a 2-hydroxybenzenethiol linker (Scheme 3). We hypothesize that the S atom in the secondary coordination sphere might facilitate the cleavage of the RS–NO bond at dicopper (I,I) and stabilize the putative $[Cu^{II}_2(NO)(SR)]^{2+}$ intermediate. Electron-donating ligands were found to stabilize copper complexes with higher oxidation states, e.g., the bis-μ-oxo-dicopper(III) isomer relative to side-on peroxo-dicopper(II) species.[34,35]

The reaction of **L** with 2 equiv of $[Cu(MeCN)_4]ONf$, $[Cu(MeCN)_4]PF_6$, or $[Cu(MeCN)_4]BAr^F_4$ affords dicopper (I,I) complexes **1** with ONf, PF_6, or BAr^F_4 counteranions in 89–97% yield (ONf = nonafluorobutanesulfonate, PF_6 = hexafluorophosphate, and BAr^F_4 = tetrakis(3,5-bis(trifluoromethyl)phenyl)borate). The treatment of **1**-BAr^F_4 with *S*-nitrosothiol $Ph^{Me}SNO$ at −60 °C in a 2:1 mixture of CH_2Cl_2 and THF affords the dark-green species **2**-BAr^F_4 (λ = 625 nm, ε = 2200 M^{-1} cm^{-1}; λ = 700 nm, ε = 2000 M^{-1} cm^{-1}, Figure 1B) that is stable below −35 °C. The UV–vis features of

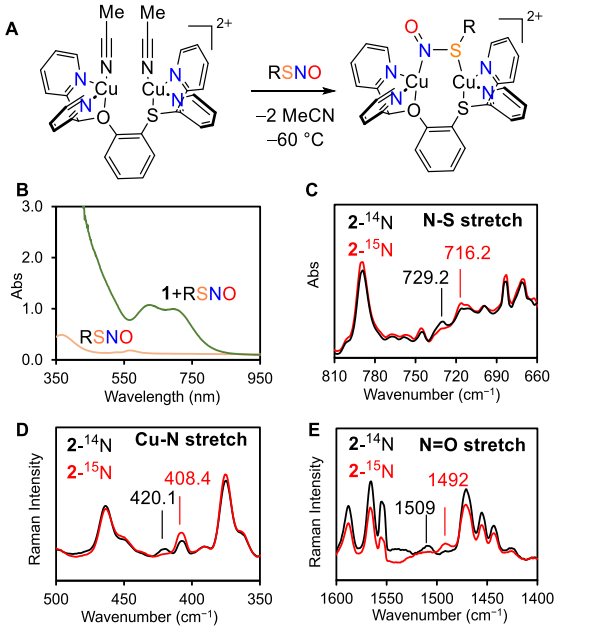

Figure 1. (A) Reaction scheme, (B) in situ UV–vis, (C) in situ IR, and (D, E) resonance Raman (568 nm excitation) spectroscopy of dicopper (I,I) *S*-nitrosothiol adduct **2**-BAr^F_4.

species **2**-BAr^F_4 closely resemble those of our previously reported dicopper(I,I) di-*S*-nitrosothiol adduct (λ = 575 nm, ε = 2400 M^{-1} cm^{-1}; λ = 675 nm, ε = 1450 M^{-1} cm^{-1}).[33] To establish the ratio of $Ph^{Me}SNO$ to the dicopper center in **2**-BAr^F_4, we performed a UV–vis titration experiment at −50 °C with dicopper(I) precursor **1**-BAr^F_4 and $Ph^{Me}SNO$. The complete conversion of **1**-BAr^F_4 to **2**-BAr^F_4 requires 1 equiv of $Ph^{Me}SNO$ (Figures S26–S28), suggesting that **2**-BAr^F_4 is a dicopper(I,I) mono-*S*-nitrosothiol adduct (Figure 1A). Consistent with this assignment, ^{15}N NMR spectroscopy of **2**-^{15}N prepared with $Ph^{Me}S^{15}NO$ at −47.9 °C shows a single ^{15}N resonance at 561.6 ppm (vs NH_3, Figure 3B).[25,33] Solution IR studies of **2** in THF or acetone display two ^{15}N-sensitive stretches at 1516(−22) cm^{-1} (N=O stretch, Figures S90 and S91) and 729 (−13) cm^{-1} (S–N stretch, Figure 1C). Resonance Raman spectra of **2**-BAr^F_4 in THF-d_8 or THF using a 568 nm excitation beam show three ^{15}N-sensitive stretches at 1509 (−18) cm^{-1}, 734 (−22) cm^{-1} (Figure S94), and 420 (−12) cm^{-1}, which were assigned as N=O, S–N, and Cu–N stretches, respectively (Figure 1D,E). The observed ^{15}N isotope shifts for the Cu–N and N–S vibrations match Hooke's law. The ^{15}N isotope shift for the N=O mode is lower than expected, likely because of coupling with additional vibrational modes. DFT models of **2** were optimized and calculated at the TPSSh/def2-TZVP/PCM(THF) level of theory. The calculated vibrational frequencies of both syn and anti isomers reproduce the experimental results reasonably well (Figure S95, Tables S7–S9).

Dicopper (I,I) *S*-nitrosothiol adduct **2** can also be generated from the treatment of **1** with 2-methylbenzenethiol ($Ph^{Me}SH$)

https://doi.org/10.1021/jacs.1c12799
J. Am. Chem. Soc. 2022, 144, 2867–2872

in the presence of excess NO• (Figures S57–S62). This reaction presumably proceeds through dicopper (II,III) μ-O μ-NO intermediate $[Cu^{II}Cu^{III}(\mu\text{-O})(\mu\text{-NO})]^{2+}$ prior to S–N bond formation,[32] as we demonstrated previously for the primary thiols.[33] The addition of 2 equiv of 2-$Ph^{Me}SH$ to **1**-BAr^F_4 or **1**-PF_6 in the presence of NO• (56 equiv) generates **2**-BAr^F_4 or **2**-PF_6 in 85 or 90% spectroscopic yield, respectively.

Despite its dark-green color in THF or acetone solution, complex **2**-BAr^F_4 crystallized as brown crystals from a mixture of pentane and THF at −40 °C. To our surprise, X-ray diffraction analysis reveals dicopper (II,II) μ-NO μ-SPh^{Me} $[Cu^{II}_2(NO)(SPh^{Me})]$ complex **3**-BAr^F_4 (Figure 2). Each Cu

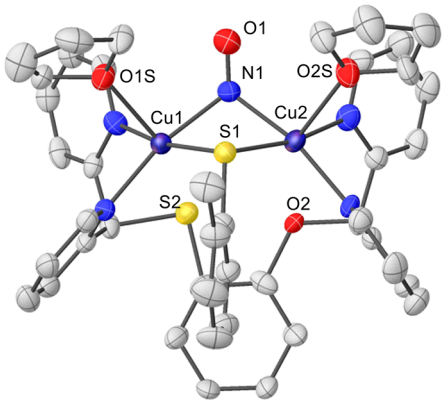

Figure 2. Single-crystal X-ray diffraction structure of complex **3**-BAr^F_4 with thermal ellipsoids at 30% probability. The BAr^F_4 counteranion and other solvent molecules are omitted for clarity. Selected bond lengths (Å) and angles (deg) for **3**-BAr^F_4: Cu1–Cu2 = 3.118(2). Cu1–N1 = 2.064(7), Cu2–N1 = 2.046(7), Cu1–S1 = 2.244(2), Cu2–S1 = 2.230(2), N1–O1 = 1.212(9), N1–S1 = 2.633(8), Cu1–N1–Cu2 = 98.7(3), and Cu1–S1–Cu2 = 88.36(8).

center binds a THF solvent molecule on the axial position to complete a square pyramidal geometry. The N=O distance is 1.212(9) Å, which is slightly longer than that in $[(XYL\text{-}O)Cu^{II}_2(\mu\text{-}NO^-)]^{2+}$ (1.176(1) Å)[36] and $[Py_4DMBCu_2(\mu\text{-}O)(\mu\text{-}NO)]^{2+}$ (1.154(19) Å).[32] Solid-state IR of **3**-BAr^F_4 (Figure S84) exhibits a ^{15}N-sensitive N=O stretch at 1530(−24) cm^{-1}, which is slightly lower than those for $[(XYL\text{-}O)Cu^{II}_2(\mu\text{-}NO^-)]^{2+}$ (1536 cm^{-1}) and $[Py_4DMBCu_2(\mu\text{-}O)(\mu\text{-}NO)]^{2+}$ (1554 cm^{-1}). Both the N=O bond distance and stretch are consistent with an NO^- formulation. No S–N stretch was detected in solid-state IR (Figure S85), consistent with the absence of an RS–NO bond in complex **3**-BAr^F_4 (N···S distance 2.633(8) Å). The reaction of **3**-BAr^F_4 with cobalt(II) porphyrin (TPP)Co in CH_2Cl_2 at −40 °C resulted in the release of 1 equiv of NO• in 79% yield (Supporting Information, Figure S75–78).

Interestingly, dissolution of the brown crystals of **3**-BAr^F_4 in a 2:1 mixture of CH_2Cl_2 and THF at −60 °C affords a dark-green solution with UV–vis features identical to those of **2**-BAr^F_4 (Figures S30 and S31), suggesting that **3**-BAr^F_4 is converted back to **2**-BAr^F_4 upon dissolution in coordinating solvents. In contrast, the dissolution of **3**-BAr^F_4 in cold CH_2Cl_2 generates a brown solution with a single UV–vis feature at 715 nm (ε = 3000 $M^{-1}cm^{-1}$), consistent with the distinct brown color of **3**-BAr^F_4 in the solid state (Figure 3A, S32). Thus, while the formation of $[Cu^I_2(RSNO)]$ **2**-BAr^F_4 is favored in coordinating solvents such as THF and acetone (Figures S29 and S45), brown isomer $[Cu^{II}_2(NO)(SR)]$ **3**-BAr^F_4 can be

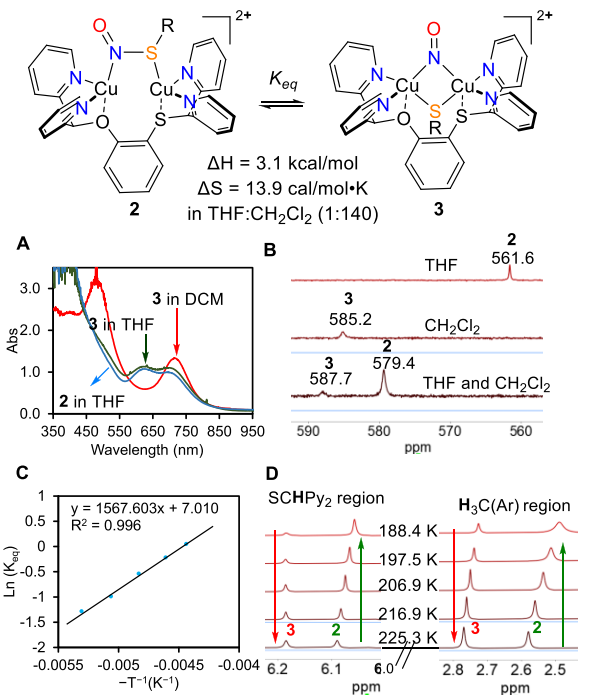

Figure 3. (A) UV–vis spectra obtained from dissolving crystals of complex **3**-BAr^F_4 in cold CH_2Cl_2 (red trace) or a 2:1 mixture of CH_2Cl_2 and THF (green trace). UV–vis spectrum of complex **2**-BAr^F_4 formed in a 2:1 mixture of CH_2Cl_2 and THF is shown in the blue trace as a comparison. (B) ^{15}NMR spectrum of **2**-BAr^F_4 in a mixture of THF-d_8/CD_2Cl_2 in 2:1 ratio (top), **3**-BAr^F_4 in CD_2Cl_2 (middle), and a mixture of **2**-BAr^F_4 and **3**-BAr^F_4 in a mixture of THF/CD_2Cl_2 in a ca. 1:18 ratio (bottom). (C) van't Hoff plot and (D) variable-temperature ^{1}H NMR data of **2**-BAr^F_4/**3**-BAr^F_4 in a mixture of THF/CD_2Cl_2 in a 1:140 ratio from 188.4 to 225.3 K.

directly generated in noncoordinating solvents such as CH_2Cl_2. The titration of $Ph^{Me}SNO$ with various amounts of **1**-PF_6 or **1**-BAr^F_4 in dichloromethane suggests that the stoichiometry of the dicopper center with respect to $Ph^{Me}SNO$ remains 1:1 in **3** (Figures S19–S24). When prepared with $Ph^{Me}S^{15}NO$, **3**-^{15}N exhibits a single ^{15}N NMR signal at 585.2 ppm, which is significantly different from **2**-^{15}N (561.6 ppm, Figure 3B). The key spectroscopic features of **2**-BAr^F_4 and **3**-BAr^F_4 are summarized in Table 1. The observation of dicopper (I,I) *S*-nitrosothiol in a coordinating solvent versus dicopper(II,II) μ-NO μ-thiolate in a noncoordinating solvent suggests that these two isomers might display a solvent-dependent interconver-

Table 1. Summary of Spectroscopic Features of 2-BAr^F_4 and 3-BAr^F_4

	IR cm^{-1}	UV-vis nm ($M^{-1}cm^{-1}$)	^{15}N NMR ppm	^{1}H NMR ppm
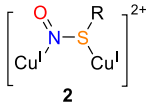 **2**	1516 N=O 729 N-S	625 (2200) 700 (2000)	561.6	2.54 H_3C(Ar) 6.08, 6.52 $HCPy_2$
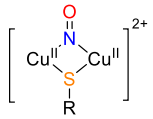 **3**	1530 N=O	715 (3000)	585.2	2.75 H_3C(Ar) 6.19, 6.53 HCPy2

https://doi.org/10.1021/jacs.1c12799
J. Am. Chem. Soc. 2022, 144, 2867–2872

sion. Indeed, the addition of THF to a dichloromethane solution of **3**-BAr^F_4 causes the gradual conversion to **2**-BAr^F_4 (Figures S34−S37). When the ratio of THF/CH_2Cl_2 reaches 1:6, **3**-BAr^F_4 cleanly converts to **2**-BAr^F_4. To further confirm that **2**-BAr^F_4 and **3**-BAr^F_4 can coexist in solution, we dissolved crystals of **3**-^{15}N in cold CD_2Cl_2 and performed ^{15}N NMR analysis at −47.9 °C. Notably, the crystals of **3**-^{15}N contain a certain amount of cocrystallized THF, which is expected to cause the partial conversion of **3**-^{15}N to **2**-^{15}N. Indeed, two distinct ^{15}N NMR signals were observed for **3**-^{15}N (587.7 ppm) and **2**-^{15}N (579.4 ppm) (Figure 3B bottom).

^{1}H NMR spectroscopy of **2**-BAr^F_4/**3**-BAr^F_4 in a 1:140 mixture of THF and CD_2Cl_2 reveals that the ratio of **2**/**3** is 0.93:1 (Figure 3D) at −47.9 °C (225.3 K). As we cooled the ^{1}H NMR sample to −84.7 °C (188.4 K), the ratio of **2**/**3** increased to 3.6:1. The construction of a van't Hoff plot using $\ln(K_{eq}) = \ln([\mathbf{3}]/[\mathbf{2}])$ vs $-1/T$ affords thermodynamic parameters for the **2** ⇌ **3** equilibrium: ΔH = 3.1 kcal/mol and ΔS = 13.9 cal/(mol K) (Figure 3C). These findings suggest that the formation of **3** is enthalpically disfavored and entropically favored.

The solvent-dependent core isomerization is reminiscent of the interconversion of μ-η^2:η^2-peroxo-[37,38] and bis(μ-oxo) dicopper complexes first observed by Tolman[39−42] and later by Karlin,[34,35,43−46] Stack,[47−50] and others[51−57] (Scheme 4A).

Scheme 4. Coordinating Solvents Favor the Cleavage of the O−O Bond and the Formation of the S−N Bond

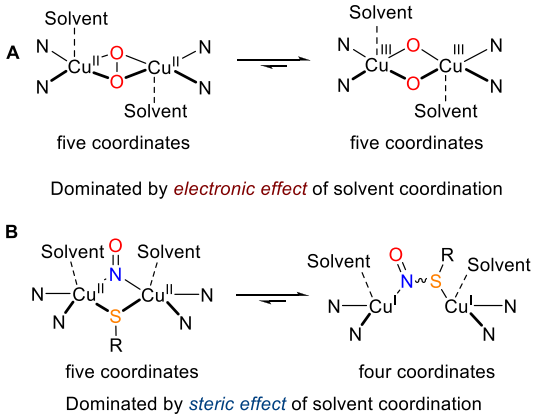

Both the reversible formation/cleavage of O−O and S−N bonds at the dicopper center shift as a function of the solvent coordination ability, albeit with opposite trends. Karlin et al. observed increasing quantities of the O−O bond cleavage product−dicopper(III,III) bis-μ-oxo complex along the series CH_2Cl_2 < Et_2O < acetone < THF.[35] The more coordinating solvents are anticipated to stabilize the formal Cu^{III} oxidation state and facilitate cleavage of the O−O bond.[35,39] In contrast, S−N bond formation is favored in solvents with greater coordinating abilities (Supporting Information, Figures S37 and S49 and Tables S1 and S2). We postulate that the coordination of solvent molecules to copper centers in complex **2** or **3** favors reductive elimination due to the dominating steric effects, as the coordination number changes from 5 in $[Cu^{II}_2(NO)(SR)]$ to 4 in $[Cu^{I}_2(RSNO)]$ (Scheme 4B). Analogous coordination-induced reductive eliminations have been observed in other Fe[58] and Cu organometallic complexes.[59,60]

We also investigated the impact of coordinating anions on the interconversion of $[Cu^{I}_2(RSNO)]$ and $[Cu^{II}_2(NO)(SR)]$. In contrast to **1**-BAr^F_4 or **1**-PF_6 (Figures S59 and S63−S66), the treatment of $Ph^{Me}SNO$ with **1**-ONf, which features a coordinating sulfonate anion, produces $[Cu^{I}_2(RSNO)]$ isomer **2**-ONf exclusively, regardless of the solvent environment (Figures S53−S55). Furthermore, $[Cu^{II}_2(NO)(SR)]$ complex **3**-BAr^F_4 can be converted to $[Cu^{I}_2(RSNO)]$ **2**-ONf upon treatment with external sulfonate source TBAONf (Supporting Information, Figures S67−S71). The coordination of sulfonate to the dicopper center promotes the formation of the S−N bond, similar to Stack et al.'s observation that O−O bond formation at the dicopper center is preferred with basic sulfonate anions.[50]

In summary, we report the first example of the controlled interconversion of RSNO and NO$^\bullet$/thiol at a metal center. The addition of *S*-nitrosothiol to a dicopper(I,I) complex in coordinating solvents affords dicopper(I,I) *S*-nitrosothiol $[Cu^{I}_2(RSNO)]$ complex **2**-BAr^F_4. The same reaction in a noncoordinating solvent produces dicopper(II,II) μ-nitrosyl μ-thiolate $[Cu^{II}_2(NO)(SR)]$ complex **3**-BAr^F_4. The equilibrium between structural isomers $[Cu^{I}_2(RSNO)]$ and $[Cu^{II}_2(NO)(SR)]$ is controlled by the temperature, solvent coordinating ability, and counterion identity. This experimental verification of the interconversion between $M_x(RSNO)$ and $M_x(NO)(SR)$ provides an important precedence that *S*-nitrosation and denitrosation can occur at the same metal site. Our ability to observe and control such an equilibrium demonstrates the sensitivity of S−N bond formation/cleavage to the local environment, which potentially explains how the direction of *S*-nitrosation vs denitrosation is regulated in space and time. A minor perturbation of the local environment, i.e., pH value, secondary coordination sphere, or hydrophobicity/hydrophilicity, could lead to a reverse in RSNO formation/decomposition. We hope that this work will motivate future studies to attempt the characterization of this important process in biological systems.

■ ASSOCIATED CONTENT

Supporting Information

The Supporting Information is available free of charge at https://pubs.acs.org/doi/10.1021/jacs.1c12799.

Experimental details, including characterization data, spectra, computational procedures and results; crystallographic data for $[LCu_2(\mu\text{-}SAr^{Me})(\mu\text{-}NO)](BAr^F_4)_2$, **3**-$BAr^F_4$ (CCDC number: 2122519) (PDF)

Accession Codes

CCDC 2122519 contains the supplementary crystallographic data for this paper. These data can be obtained free of charge via www.ccdc.cam.ac.uk/data_request/cif, or by emailing data_request@ccdc.cam.ac.uk, or by contacting The Cambridge Crystallographic Data Centre, 12 Union Road, Cambridge CB2 1EZ, UK; fax: +44 1223 336033.

■ AUTHOR INFORMATION

Corresponding Authors

Hannah S. Shafaat − *Department of Chemistry and Biochemistry and The Ohio State Biochemistry Program, The Ohio State University, Columbus, Ohio 43210, United States;* orcid.org/0000-0003-0793-4650; Email: shafaat.1@osu.edu

https://doi.org/10.1021/jacs.1c12799
J. Am. Chem. Soc. 2022, 144, 2867−2872

Shiyu Zhang − *Department of Chemistry and Biochemistry, The Ohio State University, Columbus, Ohio 43210, United States;* orcid.org/0000-0002-2536-4324; Email: zhang.8941@osu.edu

Authors

Wenjie Tao − *Department of Chemistry and Biochemistry, The Ohio State University, Columbus, Ohio 43210, United States;* orcid.org/0000-0003-3311-7793

Alina Yerbulekova − *The Ohio State Biochemistry Program, The Ohio State University, Columbus, Ohio 43210, United States*

Curtis E. Moore − *Department of Chemistry and Biochemistry, The Ohio State University, Columbus, Ohio 43210, United States;* orcid.org/0000-0002-3311-7155

Complete contact information is available at: https://pubs.acs.org/10.1021/jacs.1c12799

Notes

The authors declare no competing financial interest.

■ ACKNOWLEDGMENTS

This material is based on work supported by the U.S. National Science Foundation under award no. CHE-1904560 (S.Z.). H.S.S. acknowledges the support of the Sloan Foundation for her efforts in this work and the U.S. Department of Energy under award no. DE-SC0018020. A.Y. acknowledges the support of the U.S. Department of Energy under award no. DE-SC0018020. Tanya Whitmer and Vageesha W. Liyana Gunawardana are acknowledged for help with low-temperature NMR measurements. Jamey Bower is thanked for helpful discussions. Erica Moscarello is thanked for help with solid-state IR measurements. The authors thank The Ohio State University Department of Chemistry and Biochemistry for additional financial support.

■ REFERENCES

(1) Gow, a J.; Stamler, J. S. Reactions between Nitric Oxide and Haemoglobin under Physiological Conditions. *Nature* **1998**, *391*, 169−173.

(2) Pawloski, J. R.; Hess, D. T.; Stamler, J. S. Export by Red Blood Cells of Nitric Oxide Bioactivity. *Nature* **2001**, *409*, 622−626.

(3) Hess, D. T.; Matsumoto, A.; Kim, S.-O.; Marshall, H. E.; Stamler, J. S. Protein S-Nitrosylation: Purview and Parameters. *Nat. Rev. Mol. Cell Biol.* **2005**, *6*, 150−166.

(4) Stamler, J. S.; Jia, L.; Eu, J. P.; McMahon, T. J.; Demchenko, I. T.; Bonaventura, J.; Gernert, K.; Piantadosi, C. A. Blood Flow Regulation by *S*-Nitrosohemoglobin in the Physiological Oxygen Gradient. *Science* **1997**, *276*, 2034−2037.

(5) Iwakiri, Y.; Satoh, A.; Chatterjee, S.; Toomre, D. K.; Chalouni, C. M.; Fulton, D.; Groszmann, R. J.; Shah, V. H.; Sessa, W. C. Nitric Oxide Synthase Generates Nitric Oxide Locally to Regulate Compartmentalized Protein S-Nitrosylation and Protein Trafficking. *Proc. Natl. Acad. Sci.U.S.A.* **2006**, *103*, 19777.

(6) Williams, D. L. H. The Chemistry of S-Nitrosothiols. *Acc. Chem. Res.* **1999**, *32*, 869−876.

(7) Williams, D. L. H. *Nitrosation Reactions and the Chemistry of Nitric Oxide*; Elsevier, 2004.

(8) Williams, D. L. H. S-Nitrosation and the Reactions of S-Nitroso Compounds. *Chem. Soc. Rev.* **1985**, *14*, 171−196.

(9) Zhang, R.; Hess, D. T.; Qian, Z.; Hausladen, A.; Fonseca, F.; Chaube, R.; Reynolds, J. D.; Stamler, J. S. Hemoglobin *β*Cys93 Is Essential for Cardiovascular Function and Integrated Response to Hypoxia. *Proc. Natl. Acad. Sci. U.S.A.* **2015**, *112*, 6425.

(10) Gladwin, M. T.; Schechter, A. N.; Shelhamer, J. H.; Pannell, L. K.; Conway, D. A.; Hrinczenko, B. W.; Nichols, J. S.; Pease-Fye, M. E.; Noguchi, C. T.; Rodgers, G. P.; Ognibene, F. P. Inhaled Nitric Oxide Augments Nitric Oxide Transport on Sickle Cell Hemoglobin without Affecting Oxygen Affinity. *J. Clin. Invest.* **1999**, *104*, 937−945.

(11) Yonetani, T.; Tsuneshige, A.; Zhou, Y.; Chen, X. Electron Paramagnetic Resonance and Oxygen Binding Studies of *α*-Nitrosyl Hemoglobin: A Novel Oxygen Carrier Having NO-Assisted Allosteric Functions. *J. Biol. Chem.* **1998**, *273*, 20323−20333.

(12) Gladwin, M. T.; Wang, X.; Reiter, C. D.; Yang, B. K.; Vivas, E. X.; Bonaventura, C.; Schechter, A. N. *S*-Nitrosohemoglobin Is Unstable in the Reductive Erythrocyte Environment and Lacks O_2/NO-Linked Allosteric Function. *J. Biol. Chem.* **2002**, *277*, 27818−27828.

(13) Milanese, C.; Tapias, V.; Gabriels, S.; Cerri, S.; Levandis, G.; Blandini, F.; Tresini, M.; Shiva, S.; Greenamyre, J. T.; Gladwin, M. T.; Mastroberardino, P. G. Mitochondrial Complex I Reversible *S*-Nitrosation Improves Bioenergetics and Is Protective in Parkinson's Disease. *Antioxid. Redox Signal.* **2018**, *28*, 44−61.

(14) Boese, M.; Mordvintcev, P. I.; Vanin, A. F.; Busse, R.; Mulsch, A. *S*-Nitrosation of Serum Albumin by Dinitrosyl-Iron Complex. *J. Biol. Chem.* **1995**, *270*, 29244−29249.

(15) Vanin, A. F.; Malenkova, I. V.; Serezhenkov, V. A. Iron Catalyzes Both Decomposition and Synthesis OfS-Nitrosothiols: Optical and Electron Paramagnetic Resonance Studies. *Nitric Oxide* **1997**, *1*, 191−203.

(16) Weichsel, A.; Maes, E. M.; Andersen, J. F.; Valenzuela, J. G.; Shokhireva, T. K.; Walker, F. A.; Montfort, W. R. Heme-Assisted S-Nitrosation of a Proximal Thiolate in a Nitric Oxide Transport Protein. *Proc. Natl. Acad. Sci. U.S.A.* **2005**, *102*, 594−599.

(17) Bosworth, C. A.; Toledo, J. C.; Zmijewski, J. W.; Li, Q.; Lancaster, J. R. Dinitrosyliron Complexes and the Mechanism(s) of Cellular Protein Nitrosothiol Formation from Nitric Oxide. *Proc. Natl. Acad. Sci. U.S.A.* **2009**, *106*, 4671−4676.

(18) Poptic, A. L.; Zhang, S. Iron(II/III) Halide Complexes Promote the Interconversion of Nitric Oxide and *S*-Nitrosothiols through Reversible Fe-S Interaction. *Inorg. Chem.* **2021**, *60*, 5190−5197.

(19) Franke, A.; Stochel, G.; Suzuki, N.; Higuchi, T.; Okuzono, K.; van Eldik, R. Mechanistic Studies on the Binding of Nitric Oxide to a Synthetic Heme-Thiolate Complex Relevant to Cytochrome P450. *J. Am. Chem. Soc.* **2005**, *127*, 5360−5375.

(20) Hunt, A. P.; Lehnert, N. The Thiolate Trans Effect in Heme $\{FeNO\}^6$ Complexes and Beyond: Insight into the Nature of the Push Effect. *Inorg. Chem.* **2019**, *58*, 11317−11332.

(21) Lehnert, N.; Kim, E.; Dong, H. T.; Harland, J. B.; Hunt, A. P.; Manickas, E. C.; Oakley, K. M.; Pham, J.; Reed, G. C.; Alfaro, V. S. The Biologically Relevant Coordination Chemistry of Iron and Nitric Oxide: Electronic Structure and Reactivity. *Chem. Rev.* **2021**, *121*, 14682−14905.

(22) Inoue, K.; Akaike, T.; Miyamoto, Y.; Okamoto, T.; Sawa, T.; Otagiri, M.; Suzuki, S.; Yoshimura, T.; Maeda, H. Nitrosothiol Formation Catalyzed by Ceruloplasmin. Implication for Cytoprotective Mechanism in Vivo. *J. Biol. Chem.* **1999**, *274*, 27069−27075.

(23) Moriel, P.; Pereira, I. R. O.; Bertolami, M. C.; Abdalla, D. S. P. Is Ceruloplasmin an Important Catalyst for *S*-Nitrosothiol Generation in Hypercholesterolemia? *Free Radic. Biol. Med.* **2001**, *30*, 318−326.

(24) Tao, L.; English, A. M. Mechanism of S-Nitrosation of Recombinant Human Brain Calbindin D28K. *Biochemistry* **2003**, *42*, 3326−3334.

(25) Zhang, S.; Melzer, M. M.; Sen, S. N.; Çelebi-Ölçüm, N.; Warren, T. H. A Motif for Reversible Nitric Oxide Interactions in Metalloenzymes. *Nat. Chem.* **2016**, *8*, 663−669.

(26) Tian, S.; Liu, J.; Cowley, R. E.; Hosseinzadeh, P.; Marshall, N. M.; Yu, Y.; Robinson, H.; Nilges, M. J.; Blackburn, N. J.; Solomon, E. I.; Lu, Y. Reversible *S*-Nitrosylation in an Engineered Azurin. *Nat. Chem.* **2016**, *8*, 670−677.

(27) Wolak, M.; Stochel, G.; Van Eldik, R. Reactivity of Aquacobalamin and Reduced Cobalamin toward *S*-Nitrosoglutathione

and *S*-Nitroso-*N*-Acetylpenicillamine. *Inorg. Chem.* **2006**, *45*, 1367−1379.
(28) Richter-Addo, G. B. Binding of Organic Nitroso Compounds to Metalloporphyrins. *Acc. Chem. Res.* **1999**, *32*, 529−536.
(29) Perissinotti, L. L.; Estrin, D. A.; Leitus, G.; Doctorovich, F. A Surprisingly Stable *S*-Nitrosothiol Complex. *J. Am. Chem. Soc.* **2006**, *128*, 2512−2513.
(30) Jourd'heuil, D.; Laroux, F. S.; Miles, A. M.; Wink, D. A.; Grisham, M. B. Effect of Superoxide Dismutase on the Stability of *S*-Nitrosothiols. *Arch. Biochem. Biophys.* **1999**, *361*, 323−330.
(31) Johnson, M. A.; Macdonald, T. L.; Mannick, J. B.; Conaway, M. R.; Gaston, B. Accelerated S-Nitrosothiol Breakdown by Amyotrophic Lateral Sclerosis Mutant Copper, Zinc-Superoxide Dismutase. *J. Biol. Chem.* **2001**, *276*, 39872−39878.
(32) Tao, W.; Bower, J. K.; Moore, C. E.; Zhang, S. Dicopper μ -oxo, μ-nitrosyl Complex from the Activation of NO or Nitrite at a Dicopper Center. *J. Am. Chem. Soc.* **2019**, *141*, 10159−10164.
(33) Tao, W.; Moore, C. E.; Zhang, S. Redox-Neutral *S*-Nitrosation Mediated by a Dicopper Center. *Angew. Chem., Int. Ed.* **2021**, *60*, 15980−15987.
(34) Henson, M. J.; Vance, M. A.; Zhang, C. X.; Hong-Chang, L.; Karlin, K. D.; Solomon, E. I. Resonance Raman Investigation of Equatorial Ligand Donor Effects on the $Cu_2O_2^{2+}$ Core in End-on and Side-on μ-Peroxo-Dicopper(II) and Bis-μ-Oxo-Dicopper(III) Complexes. *J. Am. Chem. Soc.* **2003**, *125*, 5186−5192.
(35) Liang, H.-C.; Henson, M. J.; Hatcher, L. Q.; Vance, M. A.; Zhang, C. X.; Lahti, D.; Kaderli, S.; Sommer, R. D.; Rheingold, A. L.; Zuberbühler, A. D.; Solomon, E. I.; Karlin, K. D. Solvent Effects on the Conversion of Dicopper(II) μ-η^2, η^2 -Peroxo to Bis-μ-Oxo Dicopper(III) Complexes: Direct Probing of the Solvent Interaction. *Inorg. Chem.* **2004**, *43*, 4115−4117.
(36) Paul, P. P.; Tyeklar, Z.; Farooq, A.; Karlin, K. D.; Liu, S.; Zubieta, J. Isolation and X-Ray Structure of a Dinuclear Copper-Nitrosyl Complex. *J. Am. Chem. Soc.* **1990**, *112*, 2430−2432.
(37) Kitajima, N.; Fujisawa, K.; Fujimoto, C.; Moro-Oka, Y.; Hashimoto, S.; Kitagawa, T.; Toriumi, K.; Tatsumi, K.; Nakamura, A. A New Model for Dioxygen Binding in Hemocyanin. Synthesis, Characterization, and Molecular Structure of the μ-η^2:η^2 Peroxo Dinuclear Copper(II) Complexes, $[Cu(HB(3,5\text{-}R_2pz)_3)]_2(O_2)$ (R = i-Pr and Ph). *J. Am. Chem. Soc.* **1992**, *114*, 1277−1291.
(38) Mahapatra, S.; Halfen, J. A.; Wilkinson, E. C.; Que, L.; Tolman, W. B. Modeling Copper-Dioxygen Reactivity in Proteins: Aliphatic C-H Bond Activation by a New Dicopper(II)-Peroxo Complex. *J. Am. Chem. Soc.* **1994**, *116*, 9785−9786.
(39) Halfen, J. A.; Mahapatra, S.; Wilkinson, E. C.; Kaderli, S.; Young, V. G., Jr.; Que, L., Jr.; Zuberbuhler, A. D.; Tolman, W. B. Reversible Cleavage and Formation of the Dioxygen O-O Bond within a Dicopper Complex. *Science* **1996**, *271*, 1397−1400.
(40) Tolman, W. B. Making and Breaking the Dioxygen O-O Bond: New Insights from Studies of Synthetic Copper Complexes. *Acc. Chem. Res.* **1997**, *30*, 227−237.
(41) Cahoy, J.; Holland, P. L.; Tolman, W. B. Experimental Studies of the Interconversion of μ-η^2:η^2-Peroxo- and Bis(μ-Oxo)Dicopper Complexes. *Inorg. Chem.* **1999**, *38*, 2161−2168.
(42) Elwell, C. E.; Gagnon, N. L.; Neisen, B. D.; Dhar, D.; Spaeth, A. D.; Yee, G. M.; Tolman, W. B. Copper−Oxygen Complexes Revisited: Structures, Spectroscopy, and Reactivity. *Chem. Rev.* **2017**, *117*, 2059−2107.
(43) Tyeklár, Z.; Jacobson, R. R.; Wei, N.; Murthy, N. N.; Zubieta, J.; Karlin, K. D. Reversible Reaction of O2 (and CO) with a Copper(I) Complex. X-Ray Structures of Relevant Mononuclear Cu(I) Precursor Adducts and the Trans-(μ-1,2-Peroxo)Dicopper(II) Product. *J. Am. Chem. Soc.* **1993**, *115*, 2677−2689.
(44) Karlin, K. D.; Kaderli, S.; Zuberbühler, A. D. Kinetics and Thermodynamics of Copper(I)/Dioxygen Interaction. *Acc. Chem. Res.* **1997**, *30*, 139−147.
(45) Hatcher, L. Q.; Vance, M. A.; Sarjeant, A. A. N.; Solomon, E. I.; Karlin, K. D. Copper-Dioxygen Adducts and the Side-on Peroxo Dicopper(II)/Bis(μ-Oxo) Dicopper(III) Equilibrium: Significant Ligand Electronic Effects. *Inorg. Chem.* **2006**, *45*, 3004−3013.
(46) Park, G. Y.; Qayyum, M. F.; Woertink, J.; Hodgson, K. O.; Hedman, B.; Narducci Sarjeant, A. A.; Solomon, E. I.; Karlin, K. D. Geometric and Electronic Structure of $[\{Cu(MeAN)\}_2(\mu\text{-}\eta^2\text{:}\eta^2(O_2^{2-}))]^{2+}$ with an Unusually Long O-O Bond: O-O Bond Weakening vs Activation for Reductive Cleavage. *J. Am. Chem. Soc.* **2012**, *134*, 8513−8524.
(47) Stack, T. D. P. Complexity with Simplicity: A Steric Continuum of Chelating Diamines with Copper(I) and Dioxygen. *Dalt. Trans.* **2003**, *10*, 1881−1889.
(48) Mahadevan, V.; Henson, M. J.; Solomon, E. I.; Stack, T. D. P. Differential Reactivity between Interconvertible Side-On Peroxo and Bis-μ-Oxodicopper Isomers Using Peralkylated Diamine Ligands. *J. Am. Chem. Soc.* **2000**, *122*, 10249−10250.
(49) Mirica, L. M.; Ottenwaelder, X.; Stack, T. D. P. Structure and Spectroscopy of Copper-Dioxygen Complexes. *Chem. Rev.* **2004**, *104*, 1013−1046.
(50) Ottenwaelder, X.; Rudd, D. J.; Corbett, M. C.; Hodgson, K. O.; Hedman, B.; Stack, T. D. P. Reversible O-O Bond Cleavage in Copper-Dioxygen Isomers: Impact of Anion Basicity. *J. Am. Chem. Soc.* **2006**, *128*, 9268−9269.
(51) Henson, M. J.; Mukherjee, P.; Root, D. E.; Stack, T. D. P.; Solomon, E. I. Spectroscopic and Electronic Structural Studies of the $Cu(III)_2$ Bis-μ-oxo Core and Its Relation to the Side-on Peroxo-Bridged Dimer. *J. Am. Chem. Soc.* **1999**, *121*, 10332−10345.
(52) Chen, P.; Solomon, E. I. Frontier Molecular Orbital Analysis of Cu_n-O_2 Reactivity. *J. Inorg. Biochem.* **2002**, *88*, 368−374.
(53) Goswami, V. E.; Walli, A.; Förster, M.; Dechert, S.; Demeshko, S.; Holthausen, M. C.; Meyer, F. Acid/Base Triggered Interconversion of μ-η^2:η^2-Peroxido and Bis(μ-Oxido) Dicopper Intermediates Capped by Proton-Responsive Ligands. *Chem. Sci.* **2017**, *8*, 3031−3037.
(54) Wang, V. C. C.; Maji, S.; Chen, P. P. Y.; Lee, H. K.; Yu, S. S. F.; Chan, S. I. Alkane Oxidation: Methane Monooxygenases, Related Enzymes, and Their Biomimetics. *Chem. Rev.* **2017**, *117*, 8574−8621.
(55) Trammell, R.; Rajabimoghadam, K.; Garcia-Bosch, I. Copper-Promoted Functionalization of Organic Molecules: From Biologically Relevant Cu/O_2 Model Systems to Organometallic Transformations. *Chem. Rev.* **2019**, *119*, 2954−3031.
(56) Wang, C.; Zhang, Z.; Liu, W.; Zhang, Q.; Wang, X. G.; Xie, Z.; Zhou, Z. Enzyme-Inspired Room-Temperature Lithium−Oxygen Chemistry via Reversible Cleavage and Formation of Dioxygen Bonds. *Angew. Chem., Int. Ed.* **2020**, *59*, 17856−17863.
(57) Vargo, N. P.; Harland, J. B.; Musselman, B. W.; Lehnert, N.; Ertem, M. Z.; Robinson, J. R. Calcium-Ion Binding Mediates the Reversible Interconversion of Cis and Trans Peroxido Dicopper Cores. *Angew. Chem., Int. Ed.* **2021**, *60*, 19836−19842.
(58) Russell, S. K.; Lobkovsky, E.; Chirik, P. J. Iron-Catalyzed Intermolecular $[2\pi + 2\pi]$ Cycloaddition. *J. Am. Chem. Soc.* **2011**, *133*, 8858−8861.
(59) Liu, S.; Liu, H.; Liu, S.; Lu, Z.; Lu, C.; Leng, X.; Lan, Y.; Shen, Q. $C(sp^3)$-CF_3 Reductive Elimination from a Five-Coordinate Neutral Copper(III) Complex. *J. Am. Chem. Soc.* **2020**, *142*, 9785−9791.
(60) Huffman, L. M.; Stahl, S. S. Mechanistic Analysis of Trans C-N Reductive Elimination from a Square-Planar Macrocyclic Aryl-Copper(III) Complex. *Dalt. Trans.* **2011**, *40*, 8959.

https://doi.org/10.1021/jacs.1c12799
J. Am. Chem. Soc. 2022, 144, 2867−2872